Original Paper

Eletrônica de Potência
Open Journal of Power Electronics

Received July 31, 2024; accepted October 02, 2024; Date of publication October 13, 2024.
The review of this paper was arranged by Associate Editor Allan F. Cupertino and Editor-in-Chief Heverton A. Pereira.

Digital Object Identifier http://doi.org/10.18618/REP.e202438

Junction Temperature Prediction and Lifetime Assessment in a PV Inverter Using a 10-year Mission profile

Andrei C. Ribeiro[1,3], Rômullo R. M. Carvalho[1], Francisco V. E. Lemos[1,4], João P. C. Silveira[1], Pedro J. S. Neto[2], Carlos E. Beluzo[3], Tárcio A. S. Barros[1]

[1]Universidade Estadual de Campinas (UNICAMP), School of Electrical and Computer Engineering, Campinas, SP, Brazil.
[2]Universidade Estadual de Campinas (UNICAMP), School of Mechanical Engineering, Campinas, SP, Brazil.
[3]Federal Institute of São Paulo, Campinas, SP, Brazil.
[4]Federal Institute of Ceará, Mombaça, CE, Brazil.

e-mail: a223987@dac.unicamp.br, r217905@dac.unicamp.br, f224006@dac.unicamp.br, jpedrocs@unicamp.br, pedrosn@unicamp.br, beluzo@ifsp.edu.br, tarcio87@unicamp.br

ABSTRACT The expansion of great-scale photovoltaic (PV) power plants indicates the need for an accurate lifetime assessment of inverters to maintain energy supply availability. In this context, the study contributes in two ways. First, we use machine-learning (ML) models for junction temperature prediction. Second, we perform reliability assessments using a 10-year mission profile in three Brazilian cities. The thermal loadings are obtained through a look-up table approach. Although the ML models exhibit different performances in regression, other factors must be considered, such as easy-to-apply, interpretability, and generalization capability. The reliability assessment is typically based on an annual mission profile, assuming damage repeats until failure. However, only the historical series can confirm whether this choice was acceptable, pessimistic, or optimistic. For instance, in Campos do Jordão-SP, if the chosen mission profile is 2014, the expected failure of 10% of inverter samples occurs three years earlier than suggested by the historical series. Regardless of the methodology used to estimate thermal loading or accumulated damage, the mission profile significantly influences photovoltaic inverter reliability, indicating that if more data is available, the chosen mission profile should align with the historical series.

KEYWORDS Junction temperature prediction, lifetime assessment, machine-learning models, mission profile, photovoltaic inverter reliability.

I. INTRODUCTION

The generation of energy from renewable resources has increased significantly in recent years. The energy transition boosts the demand for more efficient and reliable power converters, challenging the state-of-the-art. Reliability is associated with the expected lifespan of a component, converter, or system. In other words, reliability is defined as the probability the device will continue to perform its functions without failure under specified operational or environmental conditions for a certain period [1]. Therefore, meeting this constraint becomes more difficult as the functions performed by the converter and operational conditions are even more challenging.

The expected lifespan of a photovoltaic (PV) system is commonly estimated at around 25 years. Manufacturers use such estimation as a guideline to guarantee that at least 80% of the initial generation from the PV modules will be maintained. Regarding the degradation of the modules, it is observed a generation drop between 2-3% after twelve months and approximately 0.5% in the following years [2]. On the other hand, manufacturers of photovoltaic inverters typically provide a warranty period of 5 to 10 years, indicating that failures due to aging and wear of the inverter components are likely to occur after this period [3].

The mission profile should be the basis for lifetime assessment. In the case of PV generation, irradiance and ambient temperature affect the energy produced and, consequently, the thermal stress to which the inner components are subjected [4].

Capacitors and power semiconductor switches are the components that fail most often inside a PV inverter [5]. Their lifespan is significantly affected by thermal loading, i.e., junction temperature T_j and hotspot temperature T_h [3], [6], [7]. Effective thermal management aims to maintain temperatures below their maximum limit while, even more importantly, controlling thermal loading to ensure the expected lifetime [8], [9].

The current work is an extension of article [10], where the authors previously utilized two machine-learning models to characterize the thermal loading of power switches. The target variables were the average junction temperature T_{jm} and its fluctuation ΔT_j.

This extension incorporated two additional models: an MLP (multilayer perceptron) and the XGBoost algorithm.

The latter is a cutting-edge technique and a leading choice in Kaggle competitions and real-world applications [11], [12].

Typically, reliability assessment begins with a representative annual mission profile [13], [14]. The damage accumulated over this period is calculated, and assuming the same wear and tear will be observed in subsequent years, the expected lifespan is determined. For example, if an electronic component experiences 10% damage during one year, its expected lifespan is ten years, meaning its accumulated damage has reached 100%. The previous premise simplifies the reliability assessment. However, it is impossible to determine if the year was an accurate choice with an acceptable margin of error without examining the historical data.

In energy generation, a common approach to dealing with lack of data is using a Typical Meteorological Year (TMY). Numerous studies aim to define the TMY, with data sources and methods varying from country to country, emphasizing the need for compatible and standardized databases. For instance, the work in [15] presents a TMY dataset that can be useful for reliability studies lacking meteorological data. However, the TMYs provided have a granularity of 1 hour between two samples. As presented in [16], [17], an increased sampling time provides an optimistic lifetime evaluation for power devices.

In this context, this paper also addresses the question: "*How does PV inverter reliability vary when using a one-year profile, a 10-year mission profile, or a TMY?*". To answer it, we evaluate the reliability of a PV inverter in three Brazilian cities. Fig. 1 illustrates the typical ambient temperature profile in Campos do Jordão-SP, Campinas-SP, and Teresina-PI.

The new achievements of this paper in relation to [10] can be summarized as follows:

- A more realistic system in closed-loop operation was used instead of a toy model (simplistic representation in open-loop with many details removed). However, it was necessary to use a look-up table (LUT) based approach.
- Ten years of data were split in training/test for three cities instead of just one year for one city. Moreover, two models were included.
- Reliability assessment was executed to evaluate the impact of choosing different representative years from 2014 to 2023.

The Introduction sets the stage for discussing thermal loading prediction and mission profile influence on the reliability assessment. It also presents the study's new achievements. Section II details the translation of the mission profile and Section III presents the models trained to estimate junction temperature. Section IV outlines the reliability assessment. Section V establishes the connection between both thermal loading prediction and reliability assessment. Section VI presents the results and discussions. Finally, in the Conclusion, the pros and cons of each model and the mission profile's influence are reinforced.

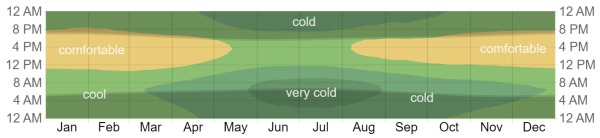

(a) Campos do Jordão-SP.

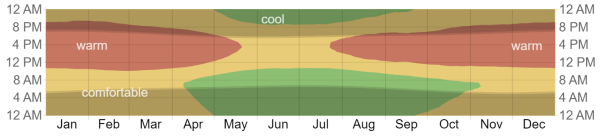

(b) Campinas-SP.

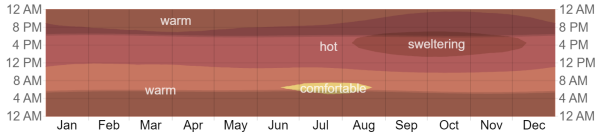

(c) Teresina-PI.

FIGURE 1. The average hourly ambient temperature (T_{amb}) [18]. ***Very cold*****: 0 °C $<$ T_{amb} $<$ 7.2 °C,** ***cold*****: 7.2 °C $<$ T_{amb} $<$ 12.8 °C,** ***cool*****: 12.8 °C $<$ T_{amb} $<$ 18.3 °C,** ***comfortable*****: 18.3 °C $<$ T_{amb} $<$ 23.9 °C,** ***warm*****: 23.9 °C $<$ T_{amb} $<$ 29.4 °C,** ***hot*****: 29.4 °C $<$ T_{amb} $<$ 35.0 °C and** ***sweltering*****: T_{amb} $>$ 35.0 °C.**

II. TRANSLATING MISSION PROFILE INTO THERMAL LOADING

The reliability assessment of components in a PV system demands processing irradiance and temperature to quantify damage over time. This is a time-consuming task that requires optimizing computational resources [4].

An efficient approach is translating a yearly mission profile into thermal loading using look-up tables (LUTs) [13], which output conduction and switching losses that serve as inputs to thermal models. This method bypasses the simulation steps required by converter controllers, streamlining the analysis process. Besides, the LUTs should include a third input - the junction temperature - as losses are related to the silicon (Si) die temperature. When generating the LUTs, the junction temperature must be fixed in at least two points. In PSIM software, this can be achieved by removing the thermal characteristics and connecting a constant voltage source with the desired junction temperature.

The LUTs will have discrete points requiring interpolation (or extrapolation) to cover the entire mission profile. In this work, tables are generated using the following arrays of irradiance (GHI), ambient temperature (T_{amb}) and junction temperature (T_{jm}):

$$\text{GHI} = (0, 200, 400, 600, 800, 1000)\ \text{[W/m²]}$$

$$T_{amb} = (-10, 10, 30, 50)\ \text{[ºC]}$$

$$T_{jm} = (25, 125)\ \text{[ºC]}$$

which results in a three-dimensional LUT with 48 points.

The system illustrated in Fig. 2 was used in the LUTs construction. The converter's main parameters and the IGBT's thermal characteristics are presented in Table 1 and 2, respectively.

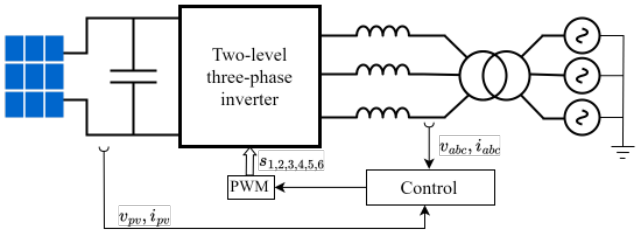

FIGURE 2. Photovoltaic system: PV array, DC link, IGBT bridge, filters, grid connection, and control.

TABLE 1. PV converter main parameters.

Parameter	Symbol	Value
Nominal power	P_n	40 kW
Switching frequency	f_{sw}	15 kHz
PV array maximum power	P_{mpp}	38 kW
PV open circuit voltage	V_{oc}	850 V
DC-link voltage reference	V_{dc}	680 V
Line-to-line grid voltage	$V_{g,l-l}$	220 Vrms
Grid frequency	f_g	60 Hz
DC-link capacitance	C_{dc}	2.35 mF
AC Filter inductance	L_f	4 mH

TABLE 2. Electrothermal description for the power module (part number: IFS150B12N3E-B31).

Parameter	Symbol	Value
Collector-emitter voltage	V_{ce}	1200 V
Nominal collector current	$I_{c,nom}$	150 A
Operating junction temperature	$T_{j,op}$	150°C
Maximum junction temperature	$T_{j,max}$	175°C
Total power dissipation	P_{tot}	750 W
IGBT J-C thermal resistance*	$R_{qth\,j-c}$	0.2 K/W
IGBT C-H thermal resistance*	$R_{qth\,c-h}$	0.083 K/W
Diode J-C thermal resistance*	$R_{dth\,j-c}$	0.375 K/W
Diode C-H thermal resistance*	$R_{dth\,c-h}$	0.155 K/W

*Per IGBT and diode

The total power P_{Tot} dissipated by a power switch, presented in (1), is obtained by summing the conduction losses P_{cond} and switching losses P_{sw} given in LUTs.

$$\text{P}_{\text{Tot}} = P_{\text{cond}} + P_{\text{sw}} \tag{1}$$

Conduction losses occur when the device is in full conduction. The current through the device $i_c(t)$ is equal to the current required for the circuit, and the voltage across its terminals $v_{ce}(t)$ is the drop due to the device itself. These losses are related to the duty cycle t_0/T. On the other hand, switching losses occur during the transition from the off-state to the on-state and vice versa. The energy dissipated $E_{\text{on+off}}$ needs to be multiplied by the switching frequency f_{sw}.

The IGBT can fail due to thermomechanical breakdown, such as bond wire lift-off or solder cracking [19]. The thermal representation of the IGBT layers is shown in Fig. 3.

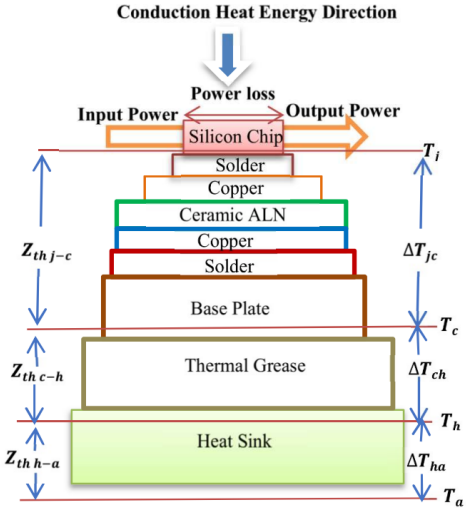

FIGURE 3. Internal structure of a semiconductor device with thermal representation [20].

Equation (2) shows how to estimate the junction temperature T_j in an IGBT whose thermal resistance from the junction to the case and from the case to the heat sink is given by $R_{qth\,j-c}$ and $R_{qth\,c-h}$, respectively. The heat sink temperature is T_h, and the average total dissipated power is equal to P_{Tot}.

$$T_j = P_{\text{Tot}} \cdot (R_{qth\,j-c} + R_{qth\,c-h}) + T_h \tag{2}$$

The estimation of junction temperature fluctuation is done using thermal impedance, which also considers the thermal capacitance. The thermal impedance is obtained from normalized curves found in datasheets of power semiconductor components. To represent the heat transfer from the heat sink to the ambient, we adopted $R_{th\,h-a}$ = 0.06 K/W, corresponding to a typical thermal resistance value with forced air cooling.

Moreover, the thermal circuit was simplified to accelerate translating the yearly mission profile into thermal loading. Although using only thermal resistances allows for a fast translation, it does not capture thermal cycling ΔT_j, a critical variable in lifetime models. To address this, we employed the two-pulse analytical method to estimate short-term thermal cycling presented in [21] and better discussed in Section IV.

III. MACHINE-LEARNING MODELS APPLIED ON MISSION PROFILE AND THERMAL LOADING

A. Linear regressor

A linear regressor is a machine-learning model that predicts a continuous target based on one or more input features. The concept behind it is to find the best-fitting straight line (or hyperplane in higher dimensions) that describes the relationship between features and the target variable [22].

For a multiple linear regression (multiple input features), the model can be represented as

$$\hat{y} = w_0 + w_1 \cdot x_1 + w_2 \cdot x_2 + ... + w_n \cdot x_n \tag{3}$$

where $\hat{y}$ is the predicted target variable, x_1, x_2, ..., x_n are the input features, w_1, w_2, ..., w_n are the corresponding weights for each feature, and w_0 is the bias (y-intercept).

The goal during the training phase is to find the optimal values for the weights w_1, w_2, ..., w_n that minimize the difference between the predicted target values $\hat{y}$ and the actual target values y.

This difference is measured using a cost function, an example is the Mean Squared Error (MSE)

$$\text{MSE} = \frac{1}{m}\sum_{i=1}^{m}(y_i - \hat{y}_i)^2 \tag{4}$$

where m is the number of training examples, y_i is the i-th actual target value sample, and $\hat{y}_i$ is the i-th predicted target value sample [22].

Equations (5) and (6) show the optimal coefficients and intercepts obtained for two linear regressor models using Teresina's mission profile, global horizontal irradiance (GHI) and ambient temperature (T_{amb}), to predict T_{jm} and ΔT_j

$$T_{jm} = 4.329 + 0.0592 \cdot \text{GHI} + 0.8276 \cdot T_{\text{amb}} \tag{5}$$

$$\Delta T_j = 0.7807 + 0.0098 \cdot \text{GHI} - 0.0315 \cdot T_{\text{amb}} \tag{6}$$

Four more linear regressor models were trained using the mission profiles of the other two cities. To predict T_{jm}, the intercept and coefficients for GHI and T_{amb} are -0.1367, 0.0589, and 0.9931 for Campos do Jordão and 0.3128, 0.0591, 0.9714 for Campinas.

As well, to predict ΔT_j, the intercept and coefficients for GHI and T_{amb} are 0.0644, 0.0098, and -0.0062 for Campos do Jordão and -0.0114, 0.0097, and -0.0027 for Campinas. Although this method is easy to use, its main limitation is assuming that the relationship between the inputs and the target variable is linear.

B. Decision tree and XGBoost

A decision tree (DT) is a machine-learning model for classification or regression tasks. It is a tree-like structure where each internal node represents a decision based on an input feature, each brand represents the outcome of that decision leading to the next node, and each leaf node represents a predicted outcome.

The goal is to create a tree that best splits the data into homogeneous subsets. This process involves selecting the best feature to split the data at each node and determining the best-split point (or threshold). Two common stopping criteria are when the tree reaches maximum depth or the minimum number of samples to split a node. An example of a decision tree used to predict junction temperature is provided in [10].

XGBoost is an open-source implementation designed to enhance the performance and speed of gradient-boosting algorithms. It sequentially builds an ensemble of weak learners, typically decision trees, to correct errors and improve prediction accuracy [12].

In Section VI, we will present that since the problem has only two features, both the decision tree and XGBoost (an ensemble model of DT) exhibited similar performance. The latter could be better utilized in a more complex problem, such as using more features or expanding the scope to predict accumulated damage, as done in [23] with two cascaded neural networks.

C. Multilayer Perceptron (MLP)

The multilayer perceptron (MLP) is an artificial neural network for classification and regression tasks. It consists of multiple layers of neurons, each connected to the neurons in the subsequent layer. The MLP contains an input layer that receives the input features, one or more hidden layers that process inputs, and an output layer that produces the final prediction [24].

Each layer in the MLP (except for the input layer) applies a transformation to its input, typically involving a weighted sum followed by a non-linear activation function. Passing input data through the network to obtain the output is called forward propagation.

The forward propagation step for the hidden layers can be expressed as:

$$\mathbf{z}^{(l)} = \mathbf{W}^{(l)}\mathbf{a}^{(l-1)} + \mathbf{b}^{(l)} \tag{7}$$

where $\mathbf{z}^{(l)}$ as the weighted sum for layer l, $\mathbf{W}^{(l)}$ as the weight matrix for layer l, $\mathbf{a}^{(l-1)}$ is the output for layer $l-1$, $\mathbf{b}^{(l)}$ as the bias vector for layer l.

The activation function ϕ is then applied to the weighted sum:

$$\mathbf{a}^{(l)} = \phi(\mathbf{z}^{(l)}) \tag{8}$$

where $\mathbf{a}^{(l)}$ is the output for layer l. ReLU, Sigmoid, and Tanh are examples of activation functions that can be applied to introduce non-linearity [24].

Combining these steps for a hidden layer:

$$\mathbf{a}^{(l)} = \phi(\mathbf{W}^{(l)}\mathbf{a}^{(l-1)} + \mathbf{b}^{(l)}) \tag{9}$$

During the training phase, the goal is to find the optimal weight matrix $\mathbf{W}$ and bias vector $\mathbf{b}$ that minimize the error between the prediction $\hat{y}$ and the actual target y. This goal is achieved through backpropagation combined with Gradient Descent.

The entire process is repeated: forward propagation, compute the loss function (4), use backpropagation, and update weight to reduce MSE over some epochs or until convergence is reached. MLPs are widely used in junction temperature prediction, such as in [23], [25], [26].

IV. RELIABILITY ASSESSMENT IN POWER ELECTRONICS

The mission profiles used in this study were acquired from the Solcast database [27] and consist of 105,120 and 105,408 samples (a 5-minute granularity) in a regular and leap year, respectively. Each sample includes values of irradiance in W/m² and ambient temperature in ºC.

After constructing the lookup tables, the mission profile can be used to convert power losses into thermal loading. The total average power losses P_{avg} (conduction + switching losses) can be applied to a thermal network (e.g., Cauer or Foster) [28].

In the Cauer network, each layer has a physical meaning, providing an accurate initial temperature estimate. However, it converges slowly, resulting in longer simulation times to reach the steady state. Contrarily, the Foster network lacks physical representation; its parameters are derived from the thermal response to a power pulse (e.g., T3STER from Siemens [29]). Despite an error in the initial estimate, the steady-state value is reached more quickly.

Given these limitations, two approaches are viable. The first uses a hybrid thermal network, leveraging both Foster and Cauer networks [30], offering a suitable junction temperature description for initial and steady-state values. The second option is a network comprising thermal resistances, yielding an average junction temperature T_{jm} profile. The junction temperature fluctuation ΔT_j can be calculated from (10), as detailed in [21].

$$\Delta T_j = P_{\text{avg}} \cdot Z_{th}\left(\frac{1}{8f_0}\right) + 2P_{\text{avg}} \cdot Z_{th}\left(\frac{1}{4f_0}\right) \qquad (10)$$

where P_{avg} denotes the total average power losses, Z_{th} represents thermal impedance, and f_0 is the grid frequency. The second option is the adopted choice in this work.

The reliability assessment of a power switch comprises other steps such as the cycle counting algorithm, the lifetime estimation model, and Miner's rule. The whole process is presented in Fig. 4.

The thermal loading is composed of two components. The first part is called short-term or fundamental frequency loading. It is formed by junction temperature mean value T_{jm} obtained by the thermal model formed by thermal resistances, ΔT_j obtained via (10), heating time defined as $t_0 = 1/(2f_0)$, and the number of cycles n_c between two samples equal to $60 \times 60 \times f_0 \times m$, where m is the number of minutes between two samples. The second part is called long-duration or low-frequency loading and carries directly only the information of T_{jm} and the sampling time T_s.

As presented in Fig. 4, short-duration loading can be directly applied to lifetime models during the calculation of accumulated damage since all necessary information is already described. On the other hand, long-duration cycling is not defined, requiring a cycle counting step.

A. Lifetime models and cycle counting algorithm

Several models are available in the literature to estimate the lifetime of power devices subjected to thermal cycling [31]. Regardless of the model adopted, the process can be summarized in two steps.

First, thermal loading cycles during device operation are counted and categorized by intensity and duration, typically using the Rainflow algorithm. We utilized MATLAB's native function *rainflow()* to analyze the long-term thermal loading in Fig. 4. However, the original *rainflow()* has some limitations, particularly in calculating the heating time (t_{on}) used in the Bayerer model. Recently, the authors of [32] introduced an improved cycle counting algorithm that accurately calculates t_{on} and removes half-cycles from the standard *rainflow()* output.

Second, the damage experienced by the component is calculated using a lifetime model. The device fails when the accumulated damage surpasses a defined threshold. This article uses the Bayerer model, also known as the CIPS 2008 model, as shown in (11) [33].

$$N_f = A \cdot (\Delta T_j)^{\beta_1} \cdot e^{\frac{\beta_2}{T_{jm}}} \cdot t_{on}^{\beta_3} \cdot I^{\beta_4} \cdot V^{\beta_5} \cdot D^{\beta_6} \qquad (11)$$

where N_f is the number of cycles to failure, A is the technology factor, β_1 to β_6 are curve fitting parameters which values are in Table 3, ΔT_j is the junction temperature oscillation, T_{jm} is the mean junction temperature, t_{on} is the heating time, I is the current per bond foot, V is the blocking voltage divided by 100, and D is the bond wire diameter.

TABLE 3. Curve fitting parameters and experimental conditions [33].

Parameter	Value	Exp. Condition
A	9.34E14	-
β_1	-4.416	45 K $\leq \Delta T_j \leq$ 150 K
β_2	1285	20ºC $\leq T_{jm} \leq$ 120ºC
β_3	-0.463	1 s $\leq t_{on} \leq$ 15 s
β_4	-0.716	3 A $\leq I_b \leq$ 23 A
β_5	-0.761	6 V $\leq V/100 \leq$ 33 V
β_6	-0.5	75 μm $\leq D \leq$ 500 μm

B. Miner's rule

In 1945, M. A. Miner popularized a rule initially proposed by A. Palmgren in 1924. This rule, known as Miner's Rule or the Palmgren-Miner linear damage hypothesis, has since become a fundamental concept in fatigue analysis. It is given by (12):

$$LC_{\text{IGBT}} = \sum_{i=1}^{j} \frac{n[i]}{N_f[i]} \qquad (12)$$

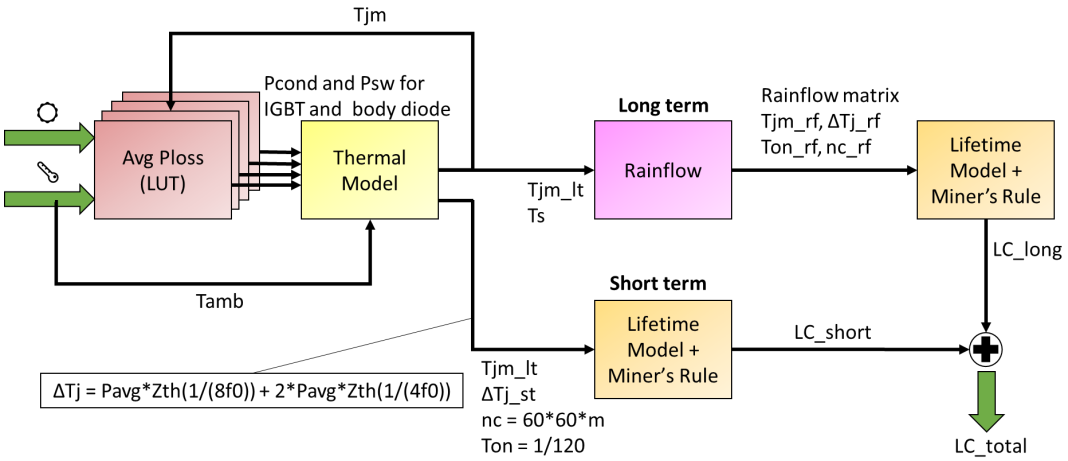

FIGURE 4. Flowchart used to compute the accumulated damage.

where LC_{IGBT} is the IGBT's lifetime consumption, $n[i]$ is the number of observed cycles and $N_f[i]$ is the expected number of cycles to failure. IGBT failure occurs when LC_{IGBT} reaches unity.

The Miner's rule in reliability assessment is based on the premise that a component will degrade linearly. In other words, the resulting thermal loading will incur damage equivalent to the summation of the calculated damage of its parts. The work in [34] presents experimental results aiming to evaluate the linear superposition premise for power modules. Additionally, seven samples of commercial power modules were subjected to thermal cycling tests. According its results, Miner's rule is aligned with the experimental behavior obtained for mixed stress conditions.

C. Monte Carlo analysis

Numerous uncertainties exist throughout the approach presented in Fig. 4, including variations in component manufacturing and different types of stress. Thus, more than a deterministic scenario is usually needed. It is critical to incorporate parametric adjustments to improve the reliability assessment.

One option is the Monte Carlo Static Parameter Method (MC-SP) [35], which estimates a histogram for lifespan rather than providing just a fixed value. In this paper, the original thermal loading is converted into an equivalent thermal loading (ETL) with static parameters $T_{jm}^{'}$ and $\Delta T_j^{'}$ in order to obtain the same damage previously calculated.

Once, there are numerous combinations of ETL. For simplicity, $t_{on}^{'}$ is defined as 0.01667s, $T_{jm}^{'}$ represents the average junction temperature of the original loading, and the number of cycles per year n_{cycles} is calculated as 365 days $\times$ 24 hours $\times$ 60 minutes $\times$ 60 seconds $\times$ 60 cycles per second.

As indicated in [13], a 3σ normal distribution variation of $\pm 20\%$ was applied in the technology factor A in (11) whose mean value was presented in Table 3. Moreover, a variation of $\pm 5\%$ following a normal distribution was adopted in $T_{jm}^{'}$ and $\Delta T_j^{'}$ [14].

D. System level reliability

Three options are available for defining how each component interacts with the system's unreliability function [36]. First, all components associated in parallel, in this case, the system fails only when all components fail. The second option is all components in series, meaning the system fails as soon as one component fails. In this case, the system's reliability will be lower (or at least equal) than the weaker component. A third option is to consider both series and parallel combined.

Considering a reliability block diagram with all components in series, the system-level unreliability function is calculated as (13):

$$U(t)_{\text{system}} = 1 - \prod_{i=1}^{n} (1 - U(t)_{i,\text{comp}}) \tag{13}$$

where U_{system} is the system's unreliability function, $U_{i,\text{comp}}$ is the unreliability function of the i-th component and n is the number of components.

Assuming that parametric variations sufficiently account for the thermal imbalance between all IGBTs, a simplified unreliability function presented in (14) can be used:

$$U(t)_{\text{system}} = 1 - (1 - U(t)_{\text{IGBT}})^6 \tag{14}$$

After obtaining the system's unreliability function, the next step is to assess it with a statistical metric, with the B_{x} being the most commonly used. In this context, x is a percentage, indicating the expected time at which x% of the PV inverter population will fail. In particular, B_1 and B_{10} are frequently employed in the industry as quality benchmarks.

V. FROM THERMAL LOADING PREDICTION TO RELIABILITY ASSESSMENT

The paper is organized into two integrated parts, presented in Sections III and IV. The first one is dedicated to translating

the mission profile into thermal loading through simulation using PSIM software and thermal models provided by power switch manufacturers. As previously discussed, this process was repeated using ten years of mission profile data for three cities. A portion of this data was used to train machine-learning (ML) models to characterize thermal loadings directly.

The second part links thermal loadings to the expected lifetime of the inverter. In addition to the thermal loadings obtained through simulation, a reliability assessment was conducted based on the thermal loadings generated by ML models. While the reliability assessment using ML models may not be more accurate than that based on the original data, it offers the advantage of not requiring specialized knowledge for future analyses. Furthermore, depending on the adopted architecture, these models can be embedded and support strategic decisions such as damage monitoring, maintenance planning, and equipment replacement.

VI. RESULTS AND DISCUSSION

The first subsection compares the performance of ML models employed for junction temperature prediction. The second subsection presents the reliability assessment results. Once the reliability assessment is applied to thermal loadings from simulation as well as from the ML models, both subsections synergize.

A. Junction temperature prediction

Before analyzing the performance of the machine-learning models used to predict junction temperature, an exploratory analysis of the problem's inputs and outputs was conducted. Boxplots were used to visualize the distribution of GHI, T_{amb}, T_j and ΔT_j in the three cities, as shown in Fig. 5 and 6.

The temperature in Campos do Jordão ranges from 2.0 °C to 34.0 °C, with 50% of the data concentrated between 16.0 °C and 22.0 °C. Campinas has a similar climate profile, with temperatures ranging from 3.0 °C to 39.0 °C and an interquartile range between 19.0 and 25.0 °C. In contrast, Teresina shows a less diverse temperature profile, with a minimum value of 19 °C and 50% of the data falling between 25.0 °C and 31.0 °C.

The interquartile range of the thermal loadings in Teresina has higher limits than the other two cities, highlighting a more significant thermal stress observed by the IGBT in this city. Since zero irradiance samples were not discarded, there is no thermal cycling (ΔT_j = 0 ºC) in half of the thermal loading. As a result, the minimum value, the first quartile, and the median of the ΔT_j boxplot are all fixed at zero.

Afterward, a correlation analysis was performed between the input features and outputs to be estimated. This analysis is illustrated in the scatter plots in Fig. 7. Irradiance has a strong (and positive) correlation with both outputs. Ambient temperature has a weaker correlation, but is still an important feature.

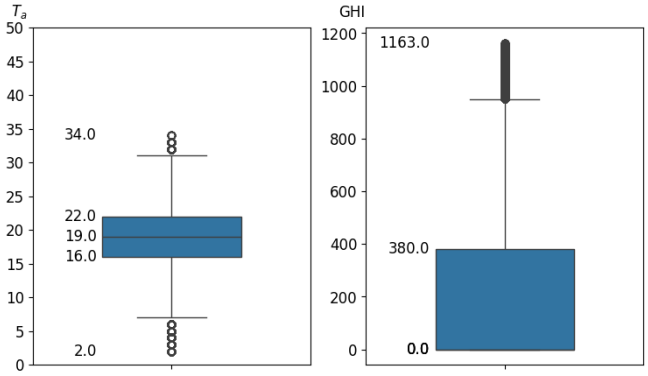

(a) The boxplot on the left shows the distribution of ambient temperature, with a 25th, 50th and 75th percentile at 16.0 °C, 19.0 °C and 22.0 °C, respectively. The boxplot on the right represents the distribution of GHI values, with a 75th percentile at 380 W/m².

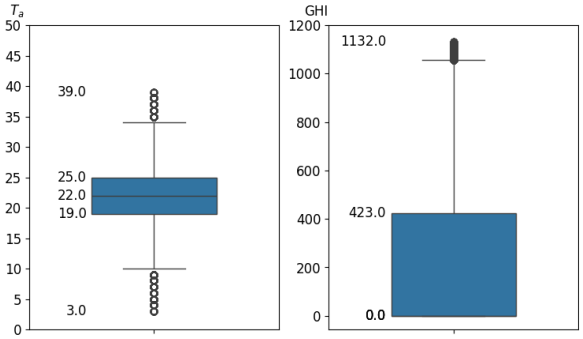

(b) The boxplot on the left shows the distribution of ambient temperature, with a 25th, 50th and 75th percentile at 19.0 °C, 22.0 °C and 25.0 °C, respectively. The boxplot on the right represents the distribution of GHI values, with a 75th percentile at 423 W/m².

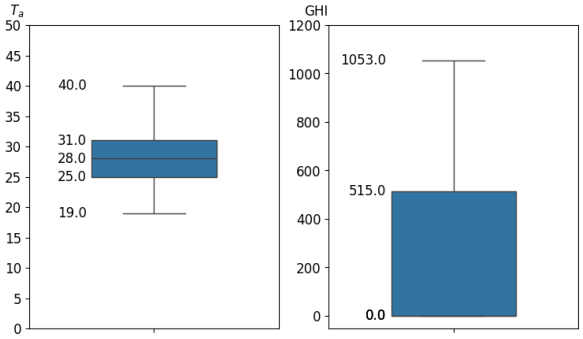

(c) The boxplot on the left shows the distribution of ambient temperature, with a 25th, 50th and 75th percentile at 25.0 °C, 28.0 °C and 31.0 °C, respectively. The boxplot on the right represents the distribution of GHI values, with a 75th percentile at 515 W/m².

FIGURE 5. Boxplots considering the mission profile from 2014 to 2023 in (a) Campos do Jordão-SP, (b) Campinas-SP, and (c) Teresina-PI.

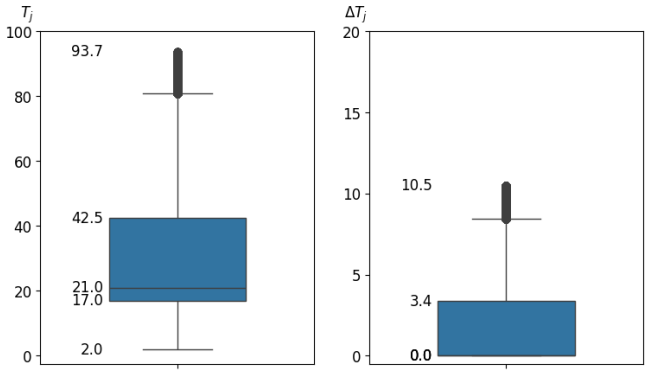

(a) The boxplot on the left represents the distribution of T_j values, with a median of 21.0 ºC, an interquartile range between 17.0 ºC and 42.5 ºC. The boxplot on the right shows the distribution of ΔT_j values, with a 75th percentile at 3.4 ºC.

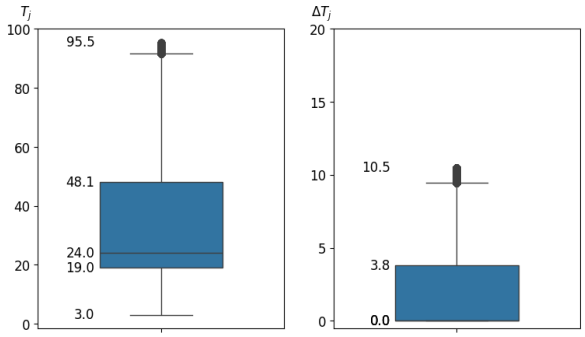

(b) The boxplot on the left represents the distribution of T_j values, with a median of 24.0 °C and an interquartile range between 19.0 °C and 48.1 °C. The boxplot on the right shows the distribution of ΔT_j values, with a 75th percentile at 3.8 °C.

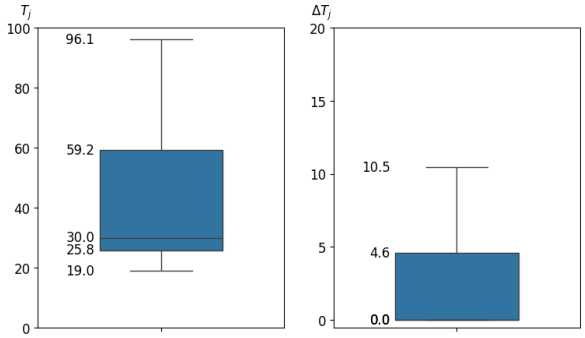

(c) The boxplot on the left represents the distribution of T_j values, with a median of 30.0 °C and an interquartile range between 25.8 °C and 59.2 °C. The boxplot on the right shows the distribution of ΔT_j values, with a 75th percentile at 4.6 °C.

FIGURE 6. Boxplots considering the thermal loadings obtained from 2014 to 2023 in (a) Campos do Jordão-SP, (b) Campinas-SP, and (c) Teresina-PI.

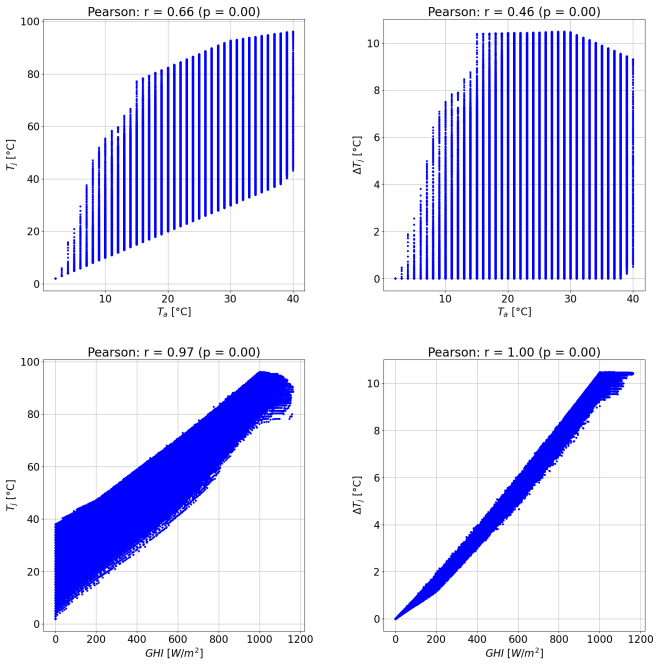

FIGURE 7. Correlation between the input and the output variables. The top row shows the correlation of thermal loading variables with T_{amb}. The bottom row shows the correlation of T_j and ΔT_j with GHI.

Except for XGBoost which has a particular library, the models used, as in [10], were implemented using the scikit-learn library.

Figures 8 and 9 show that each model's training MSE is slightly lower than its test MSE, except for the linear regressor, indicating a similar generalization capacity for training and test data. The linear model shows the highest MSE due to its inability to map non-linearities. The other models exhibit similar MSE, with the decision tree model having the lowest. Since the decision tree was the best model up to this stage, additional robustness analyses were conducted only on it.

The decision tree MSE was evaluated for the test in the same city where it was trained and in scenarios with different cities in training and testing. In this context, Fig. 10 presents some results to verify robustness.

It is worth noting that the models trained with data from Teresina map T_j and ΔT_j with greater accuracy only for Teresina with a MSE of 0.14×10^{-4}, when applied to Campinas or Campos do Jordão, the MSE observed was 3.97×10^{-4} and 8.66×10^{-4}, respectively.

On the other hand, the models trained with data from Campinas and Campos do Jordão share a reciprocal performance, as training with data from cities with well-defined seasons (or a wider range of temperatures throughout the year) benefits the generalization in the model's learning.

It has been found that ML models benefit significantly when trained on mission profiles that encompass a wide range of climatic conditions. Training them using data from

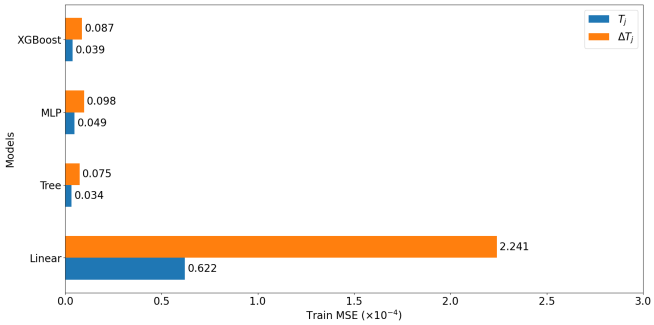

(a) Performance at the end of the training in Campos do Jordão-SP.

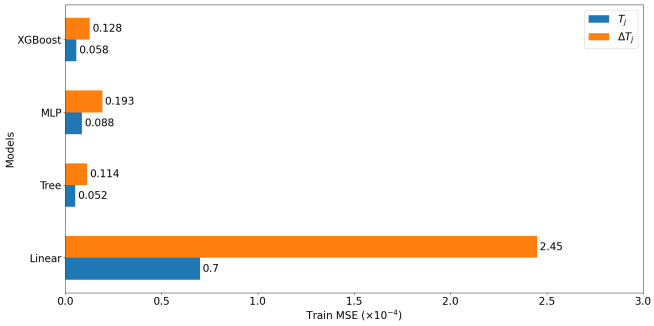

(b) Performance at the end of the training in Campinas-SP.

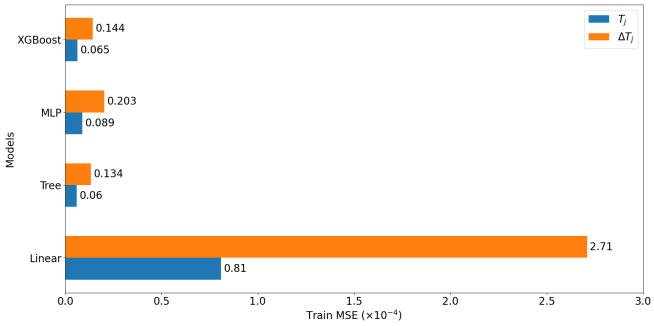

(c) Performance at the end of the training in Teresina-PI.

FIGURE 8. MSE during training.

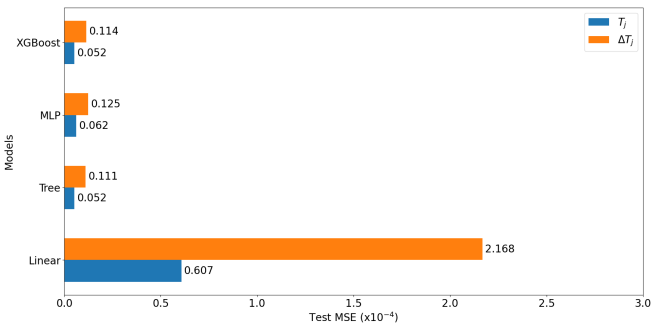

(a) Prediction performance in Campos do Jordão-SP.

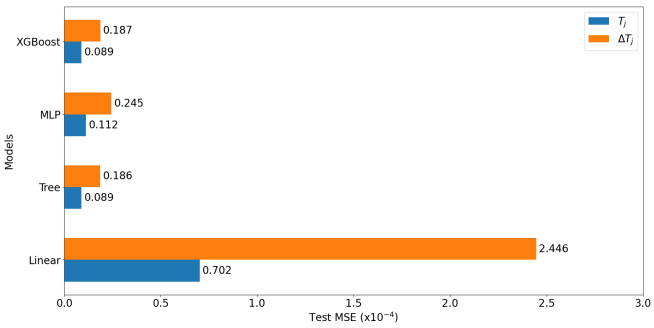

(b) Prediction performance in Campinas-SP.

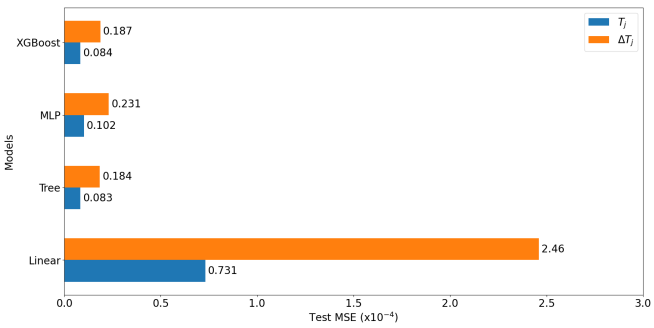

(c) Prediction performance in Teresina-PI.

FIGURE 9. MSE during test.

different cities with diverse climates can also enhance their predictive capabilities. This approach allows the models to better account for variations across geographical locations, reducing prediction errors when applied to new data.

Several strategies can reduce MSE. For same-location training and testing, techniques like Principal Component Analysis (PCA) or outlier detection algorithms, such as Local Outlier Factor (LOF), can improve generalization by filtering discrepancies. For different cities, increasing data variability and using combined mission profiles enhance model generalization. Regularization methods like dropout in MLPs can also help reduce testing MSE further [37].

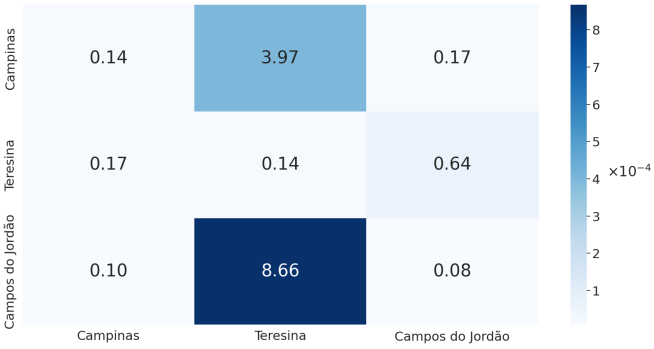

FIGURE 10. MSE of the decision tree model used when trained and tested in the same city versus different cities.

B. Reliability assessment

Tables 4, 5, and 6 show the expected lifetime in the three investigated cities. The expected lifetime for each mission profile is presented and compared with the historical period from 2014 to 2023. The static lifetime for one IGBT was 21.5, 17.6, and 14.9 years in Campos do Jordão, Campinas, and Teresina, respectively.

The highlighted rows show the years with the closest response within the historical period, making them the best candidates for representative years. For instance, choosing 2020 as the mission profile for Campos do Jordão, 2019 for Campinas, and 2014 or 2016 for Teresina ensures a response compatible with the historical period. Moreover, it facilitates data processing and reduces computational effort for further analysis.

On the other hand, 2014 in Campos do Jordão showed a damage rate of 5.85%, i.e., a failure is expected in 17.1 years, which results in a static assessment that is 4.4 years more pessimistic than the entire period's result. Considering system-level, the difference is around three years in B_{10} analysis. In addition, within the historical series, Teresina had the lowest standard deviation (σ = 1.08) among the three cities.

TABLE 4. Static lifetime, B_1 and B_{10} for one and six IGBTs (inverter level) in Campos do Jordão from 2014 to 2023. The decision tree was used to provide the thermal loading for 2020, and then the reliability assessment was executed.

Period	IGBT			Six IGBTs	
	Static lifetime	B_1	B_{10}	B_1	B_{10}
2014	17.1 y	11.5 y	14.4 y	9.6 y	12.1 y
2015	22.5 y	15.0 y	19.0 y	12.6 y	15.9 y
2016	20.3 y	13.6 y	17.1 y	11.3 y	14.3 y
2017	20.4 y	13.6 y	17.2 y	11.4 y	14.4 y
2018	25.6 y	17.1 y	21.6 y	14.3 y	18.0 y
2019	20.8 y	13.9 y	17.5 y	10.3 y	14.6 y
2020	21.9 y	14.6 y	18.4 y	12.2 y	15.4 y
2020 (DT)	21.8 y	14.5 y	18.4 y	12.2 y	15.4 y
2021	22.4 y	14.9 y	18.8 y	12.5 y	15.8 y
2022	23.9 y	16.0 y	20.2 y	13.4 y	16.9 y
2023	22.4 y	15.0 y	18.9 y	12.5 y	15.8 y
TMY (ZOH)	26.7 y	17.8 y	22.4 y	15.0 y	18.8 y
TMY (FOH)	27.9 y	18.6 y	23.4 y	15.6 y	19.6 y
2014 to 2023	21.5 y	14.4 y	18.1 y	10.5 y	15.2 y

TABLE 5. Deterministic (or static) lifetime, B_1 and B_{10} for one and six IGBTs (inverter level) in Campinas - SP from 2014 to 2023. The decision tree was used to provide the thermal loading for 2019, and then the reliability assessment was executed.

Period	IGBT			Six IGBTs	
	Static lifetime	B_1	B_{10}	B_1	B_{10}
2014	15.2 y	10.2 y	12.8 y	8.5 y	10.7 y
2015	18.8 y	12.6 y	15.8 y	10.5 y	13.3 y
2016	16.3 y	10.9 y	13.7 y	9.1 y	11.5 y
2017	17.2 y	11.5 y	14.5 y	9.6 y	12.1 y
2018	19.3 y	13.0 y	16.3 y	10.9 y	13.7 y
2019	17.7 y	11.8 y	14.9 y	9.8 y	12.4 y
2019 (DT)	17.6 y	11.8 y	14.9 y	9.8 y	12.4 y
2020	17.1 y	11.5 y	14.4 y	9.6 y	12.1 y
2021	17.3 y	11.5 y	14.5 y	9.6 y	12.2 y
2022	18.5 y	12.3 y	15.5 y	10.3 y	13.0 y
2023	18.0 y	12.0 y	15.1 y	10.0 y	12.7 y
TMY (ZOH)	22.8 y	15.2 y	19.2 y	12.8 y	16.2 y
TMY (FOH)	25.2 y	16.9 y	21.2 y	14.3 y	17.8 y
2014 to 2023	17.6 y	11.7 y	14.9 y	9.8 y	12.4 y

TABLE 6. Static lifetime, B_1 and B_{10} for one and six IGBTs (inverter level) in Teresina - PI from 2014 to 2023. The decision tree was used to provide the thermal loading for 2014 and 2016, and then the reliability assessment was executed.

Period	IGBT			Six IGBTs	
	Static lifetime	B_1	B_{10}	B_1	B_{10}
2014	14.5 y	9.7 y	12.2 y	8.1 y	10.2 y
2014 (DT)	14.6 y	9.7 y	12.3 y	8.2 y	10.3 y
2015	13.2 y	8.8 y	11.1 y	7.4 y	9.3 y
2016	14.5 y	9.7 y	12.2 y	8.1 y	10.2 y
2016 (DT)	14.5 y	9.7 y	12.2 y	8.1 y	10.2 y
2017	13.6 y	9.1 y	11.4 y	7.6 y	9.6 y
2018	15.7 y	10.4 y	13.2 y	8.7 y	11.0 y
2019	15.7 y	10.5 y	13.2 y	8.8 y	11.1 y
2020	15.4 y	10.2 y	12.9 y	8.6 y	10.8 y
2021	16.7 y	11.1 y	14.1 y	9.3 y	11.8 y
2022	15.6 y	10.4 y	13.2 y	8.8 y	11.1 y
2023	15.6 y	10.4 y	13.2 y	8.7 y	11.0 y
TMY (ZOH)	21.4 y	14.3 y	18.0 y	12.0 y	15.1 y
TMY (FOH)	22.9 y	15.3 y	19.4 y	12.8 y	16.2 y
2014 to 2023	14.9 y	10.0 y	12.5 y	8.4 y	10.5 y

The decision tree (DT), whose results were presented in the previous subsection, was used as a surrogate approach to characterize the annual thermal loading for each city's representative year. The DT thermal loadings were then utilized to assess the reliability of the inverters.

To sum up, the results in Tables 4, 5, and 6 show both the effect of a year-to-year mission profile on the lifetime prediction of a PV inverter and a similar assessment between the thermal loadings from simulation and from an ML-based approach.

Last, the expected lifetime from the TMY provided in [15] was evaluated. As previously described, originally, it had a one-hour granularity that was adjusted using zero-order hold (ZOH) and first-order hold (FOH) oversampling methods to match the 5-minute granularity of the Solcast mission profile. However, both methods do not provide enough details (fluctuations) to obtain an acceptable result [16], [17].

Therefore, a priori, this kind of TMY should only be used for reliability assessment in power devices when mission profiles with acceptable granularity are lacking.

VII. CONCLUSION

The models used for junction temperature prediction, including linear regressor, decision tree (DT), MLP, and XGBoost, demonstrated varying accuracy and interpretability. In terms of MSE, the decision tree was the best-performing one. Furthermore, the analysis showed that the DT models trained on data from cities with well-defined seasonal variations, like Campos do Jordão and Campinas, achieved better generalization and lower prediction errors when applied to different locations. The paper also investigates the variation of the reliability assessment from year to year, considering a mission profile data span of 10 years and the difference between the classical and an ML-based approach in the representative year. Considering deterministic lifetime, Campos do Jordão exhibited the highest variability in results. In system-level, Teresina, with its more harsh climate conditions, recorded an expected lifetime near to a decade in B_{10} investigation. For future works, one potential route for improving the generalization is to train models on hybrid mission profiles, for instance, using pre-selected cities with climatic conditions closely representing specific regions or biomes. On the other hand, the diversity introduced by the training set may not provide sufficient information to prevent overfitting. Techniques such as dropout in neural networks could address this and ensure better generalization also in the testing phase.

ACKNOWLEDGMENT

This study was financed in part by the Coordenação de Aperfeiçoamento de Pessoal de Nível Superior – Brasil (CAPES) – Finance Code 001 and in part by TotalEnergies / CEPETRO under FUNCAMP / UNICAMP agreement 6002.4. The authors would like to thank the late Prof. Marcelo Gradella Villalva (1978-2023) for the knowledge he passed on about photovoltaic solar energy, electric machines and power electronics, for his hard work in designing the Laboratory of Energy and Photovoltaic Systems (LESF-MV) at UNICAMP, and for all the funding he helped secure for research projects.

AUTHOR'S CONTRIBUTIONS

RIBEIRO, A.C.: Conceptualization, Data Curation, Formal Analysis, Investigation, Methodology, Simulation, Visualization, Writing - Original Draft. **CARVALHO, R.R.M.:** Data Curation, Formal Analysis, Simulation, Visualization, Writing - Original Draft. **LEMOS, F.V.E.:** Formal Analysis, Simulation. **SILVEIRA, J.P.C.:** Formal Analysis, Supervision. **NETO, P.J.S.:** Formal Analysis, Supervision. **BELUZO, C.E.:** Formal Analysis, Supervision. **BARROS, T.A.S:** Formal Analysis, Supervision, Funding Acquisition, Project Administration, Resources.

PLAGIARISM POLICY

This article was submitted to the similarity system provided by Crossref and powered by iThenticate – Similarity Check.

REFERENCES

[1] M. Modarres, K. Groth, *Reliability and risk analysis*, CRC Press, 2023.

[2] M. Chen, A. Sangwongwanich, D. Zhou, F. Blaabjerg, "Reliability Assessment of NPC inverters in PV Systems under Power Degradation and Over-Temperature Derating Operation", *in 2023 IEEE 14th International Symposium on Power Electronics for Distributed Generation Systems (PEDG)*, pp. 54–60, 2023, doi:10.1109/PEDG56097.2023.10215265.

[3] P. Hacke, S. Lokanath, P. Williams, A. Vasan, P. Sochor, G. Tamizh-Mani, H. Shinohara, S. Kurtz, "A status review of photovoltaic power conversion equipment reliability, safety, and quality assurance protocols", *Renewable and Sustainable Energy Reviews*, vol. 82, pp. 1097–1112, 2 2018, doi:10.1016/j.rser.2017.07.043, URL: https://linkinghub.elsevier.com/retrieve/pii/S1364032117311103.

[4] A. Sangwongwanich, H. Wang, F. Blaabjerg, "Reduced-Order Thermal Modeling for Photovoltaic Inverters Considering Mission Profile Dynamics", *IEEE Open Journal of Power Electronics*, vol. 1, pp. 407–419, 2020, doi:10.1109/OJPEL.2020.3025632.

[5] I. Vernica, K. Ma, F. Blaabjerg, "Optimal Derating Strategy of Power Electronics Converter for Maximum Wind Energy Production with Lifetime Information of Power Devices", *IEEE Journal of Emerging and Selected Topics in Power Electronics*, vol. 6, no. 1, pp. 267–276, 2018, doi:10.1109/JESTPE.2017.2745714.

[6] H. Wang, M. Liserre, F. Blaabjerg, "Toward reliable power electronics: Challenges, design tools, and opportunities", *IEEE Industrial Electronics Magazine*, vol. 7, pp. 17–26, 2013, doi:10.1109/MIE.2013.2252958.

[7] A. Golnas, "PV system reliability: An operator's perspective", *IEEE Journal of Photovoltaics*, vol. 3, pp. 416–421, 2013, doi:10.1109/JPHOTOV.2012.2215015.

[8] E. Laloya, O. Lucia, H. Sarnago, J. M. Burdio, "Heat Management in Power Converters: From State of the Art to Future Ultrahigh Efficiency Systems", *IEEE Transactions on Power Electronics*, vol. 31, pp. 7896–7908, 11 2016, doi:10.1109/TPEL.2015.2513433, URL: http://ieeexplore.ieee.org/document/7368925/.

[9] J. Kuprat, C. H. van der Broeck, M. Andresen, S. Kalker, M. Liserre, R. W. D. Doncker, "Research on Active Thermal Control: Actual Status and Future Trends", *IEEE Journal of Emerging and Selected Topics in Power Electronics*, vol. 9, pp. 6494–6506, 12 2021, doi:10.1109/JESTPE.2021.3067782, URL: https://ieeexplore.ieee.org/document/9382287/.

[10] A. C. Ribeiro, R. R. M. Carvalho, F. V. E. Lemos, P. J. dos S. Neto, T. A. S. Barros, M. G. Villalva, "Junction Temperature Prediction: A Multi-Featured Dataset Approach", *in 2023 IEEE 8th Southern Power Electronics Conference and 17th Brazilian Power Electronics Conference (SPEC/COBEP)*, pp. 1–8, 2023, doi:10.1109/SPEC56436.2023.10407335.

[11] K. Banachewicz, L. Massaron, *The Kaggle Book: Data analysis and machine learning for competitive data science*, Packt Publishing Ltd, 2022.

[12] C. Wade, K. Glynn, *Hands-On Gradient Boosting with XGBoost and scikit-learn: Perform accessible machine learning and extreme gradient boosting with Python*, Packt Publishing Ltd, 2020.

[13] E. M. da Silveira Brito, *Lifetime evaluation of photovoltaic inverters with capability of reactive power support*, Phd thesis, Federal University of Minas Gerais, August 2021, available at https://repositorio.ufmg.br/handle/1843/38593.

[14] A. Sangwongwanich, Y. Yang, D. Sera, F. Blaabjerg, "Lifetime Evaluation of Grid-Connected PV Inverters Considering Panel Degradation Rates and Installation Sites", *IEEE Transactions on Power Electronics*, vol. 33, pp. 1225–1236, 2 2018, doi:10.1109/TPEL.2017.2678169, URL: http://ieeexplore.ieee.org/document/7870691/.

[15] Y. Wu, J. An, C. Gui, C. Xiao, D. Yan, "A global typical meteorological year (TMY) database on ERA5 dataset", *Building Simulation*, vol. 16, pp. 1013–1026, 6 2023, doi:10.1007/s12273-023-1015-3, URL: https://link.springer.com/10.1007/s12273-023-1015-3.

[16] R. Silva, R. de Barros, E. Brito, W. Boaventura, A. Cupertino, H. Pereira, "Pursuing computationally efficient wear-out prediction of

PV inverters: The role of the mission profile resolution", *Microelectronics Reliability*, vol. 110, p. 113679, 2020.

[17] I. Vernica, H. Wang, F. Blaabjerg, "Impact of Long-Term Mission Profile Sampling Rate on the Reliability Evaluation of Power Electronics in Photovoltaic Applications", *in 2018 IEEE Energy Conversion Congress and Exposition (ECCE)*, pp. 4078–4085, 2018, doi:10.1109/ECCE.2018.8558092.

[18] WeatherSpark, "Compare the Climate and Weather in Teresina, Campinas, and Campos do Jordão", Accessed on July 6th, 2024, URL: https://weatherspark.com/compare/y/30735~30197~30407/Comparison-of-the-Average-Weather-in-Teresina-Campinas-and-Campos-do-Jordo.

[19] C. Tu, H. Xu, B. Xiao, J. Lu, Q. Guo, L. Long, "Research on the Influence of Bond Wire Lift-Off Position on the Electro-Thermal Characteristics of IGBT", *IEEE Transactions on Electron Devices*, vol. 69, no. 3, pp. 1271–1278, 2022, doi:10.1109/TED.2022.3140689.

[20] S. Bouguerra, K. Agroui, O. Gassab, A. Sangwongwanich, F. Blaabjerg, "Lifetime Estimation and Reliability of PV Inverter With Multi-Timescale Thermal Stress Analysis", *in 2019 International Aegean Conference on Electrical Machines and Power Electronics (ACEMP) & 2019 International Conference on Optimization of Electrical and Electronic Equipment (OPTIM)*, pp. 402–408, 2019, doi:10.1109/ACEMP-OPTIM44294.2019.9007221.

[21] K. Ma, F. Blaabjerg, "Reliability-cost models for the power switching devices of wind power converters", *in 2012 3rd IEEE International Symposium on Power Electronics for Distributed Generation Systems (PEDG)*, pp. 820–827, 2012, doi:10.1109/PEDG.2012.6254096.

[22] A. Géron, *Hands-on machine learning with Scikit-Learn, Keras, and TensorFlow*, " O'Reilly Media, Inc.", 2022.

[23] T. Dragicevic, P. Wheeler, F. Blaabjerg, "Artificial Intelligence Aided Automated Design for Reliability of Power Electronic Systems", *IEEE Transactions on Power Electronics*, vol. 34, pp. 7161–7171, 8 2019, doi:10.1109/TPEL.2018.2883947.

[24] S. Haykin, *Neural networks and learning machines*, Pearson Education India, 2009.

[25] Y. Yuan, L. Yunfei, W. Yang, "Online Junction Temperature Estimation System for IGBT Based on BP Neural Network", *2022 IEEE 5th International Conference on Electronics Technology (ICET)*, pp. 526–531, 5 2022, doi:10.1109/ICET55676.2022.9824077, URL: https://ieeexplore.ieee.org/document/9824077/.

[26] Y. Dou, "An Improved Prediction Model of IGBT Junction Temperature Based on Backpropagation Neural Network and Kalman Filter", *Complexity*, vol. 2021, pp. 1–10, 2 2021, doi:10.1155/2021/5542889, URL: https://www.hindawi.com/journals/complexity/2021/5542889/.

[27] Solcast, "Historical Time Series Request", Accessed on March 27th, 2024, URL: https://toolkit.solcast.com.au/historical/timeseries/request.

[28] M. Xu, K. Ma, B. Liu, X. Cai, "Modeling and Correlation of Two Thermal Paths in Frequency-Domain Thermal Impedance Model of Power Module", *IEEE Journal of Emerging and Selected Topics in Power Electronics*, vol. 9, no. 4, pp. 3971–3981, 2021, doi:10.1109/JESTPE.2020.3034574.

[29] Siemens, "Simcenter Micred T3STER", https://plm.sw.siemens.com/en-US/simcenter/physical-testing/t3ster/, accessed: April 2024, 2024.

[30] K. Ma, M. Liserre, F. Blaabjerg, T. Kerekes, "Thermal Loading and Lifetime Estimation for Power Device Considering Mission Profiles in Wind Power Converter", *IEEE Transactions on Power Electronics*, vol. 30, no. 2, pp. 590–602, 2015, doi:10.1109/TPEL.2014.2312335.

[31] F. Hosseinabadi, S. Chakraborty, S. K. Bhoi, G. Prochart, D. Hrvanovic, O. Hegazy, "A Comprehensive Overview of Reliability Assessment Strategies and Testing of Power Electronics Converters", *IEEE Open Journal of Power Electronics*, vol. 5, pp. 473–512, 2024, doi:10.1109/OJPEL.2024.3379294.

[32] R. O. De Sousa, R. C. De Barros, W. C. S. Amorim, A. F. Cupertino, H. A. Pereira, "Modified Rainflow Algorithm for Lifetime Estimation of Semiconductors Devices", *in 2023 IEEE 8th Southern Power Electronics Conference and 17th Brazilian Power Electronics Conference (SPEC/COBEP)*, pp. 1–8, 2023, doi:10.1109/SPEC56436.2023.10408046.

[33] R. Bayerer, T. Herrmann, T. Licht, J. Lutz, M. Feller, "Model for Power Cycling lifetime of IGBT Modules - various factors influencing lifetime", *in 5th International Conference on Integrated Power Electronics Systems*, pp. 1–6, 2008.

[34] M. Hernes, S. D'Arco, O. C. Spro, D. Peftitsis, "Experimental Validation of Linear Damage Superposition for IGBT Power Modules Under High and Low Temperature Stress Cycles", *in PCIM Europe digital days 2021; International Exhibition and Conference for Power Electronics, Intelligent Motion, Renewable Energy and Energy Management*, pp. 1–6, 2021.

[35] M. Novak, A. Sangwongwanich, F. Blaabjerg, "Monte Carlo-Based Reliability Estimation Methods for Power Devices in Power Electronics Systems", *IEEE Open Journal of Power Electronics*, vol. 2, pp. 523–534, 2021, doi:10.1109/OJPEL.2021.3116070.

[36] H. S.-h. Chung, H. Wang, F. Blaabjerg, M. Pecht, *et al.*, *Reliability of power electronic converter systems*, Institution of Engineering and Technology Stevenage, UK, 2015.

[37] N. Srivastava, G. Hinton, A. Krizhevsky, I. Sutskever, R. Salakhutdinov, "Dropout: A Simple Way to Prevent Neural Networks from Overfitting", *Journal of Machine Learning Research*, vol. 15, no. 56, pp. 1929–1958, 2014, URL: http://jmlr.org/papers/v15/srivastava14a.html.

BIOGRAPHIES

Andrei C. Ribeiro holds a Bachelor's (2017) and a Master's degree (2019) in Electrical Engineering from the Federal University of Piauí (UFPI). Additionally, between 2020 and 2021, he worked as a professor at UFPI. Currently, he is a Ph.D. candidate at UNICAMP, conducting research about reliability assessment in photovoltaic inverters.

Rômullo R. M. Carvalho holds a Bachelor's (2017) and a Master's degree (2020) in Electrical Engineering from UFPI. Currently, he is a Ph.D. student in Electrical Engineering at UNICAMP, conducting research about computer vision and machine-learning.

Francisco V. E. Lemos holds a Bachelor's (2017) and a Master's degree (2020) in Electrical Engineering from UFPI. Currently, he is a full-time professor at IFCE and a Ph.D. student at UNICAMP.

João P. C. Silveira holds a Bachelor's (2013) and Master's (2016) in Electrical Engineering at UnB. In 2017, he began his Ph.D. at UNICAMP, completing it in January 2022. Afterward, he completed a postdoctoral fellowship at the Faculty of Mechanical Engineering (FEM) at UNICAMP in partnership with INGETEAM, concluding in 2023. Currently, he is a collaborating professor at the Faculty of Electrical and Computer Engineering (FEEC) and a postdoctoral researcher at the Center for Energy and Petroleum Studies (CEPETRO) in partnership with Total Energies.

Pedro J. S. Neto is an MS.3-1 Professor at the School of Mechanical Engineering (UNICAMP). He holds a Ph.D. in Electrical Engineering from UNICAMP and a Bachelor's degree in Electrical Engineering from the Federal University of Vale do São Francisco. In 2019, he was a visiting Ph.D. student (BEPE/FAPESP) at Aalborg University, Denmark. He is a member of SOBRAEP, SBA, and IEEE.

Carlos E. Beluzo is a full-time professor at IFSP Campus Campinas in the area of Programming and Databases. He holds a Bachelor's degree in Computer Science from ICMC/USP, a Master's degree in Mechanical Engineering from EESC/USP, and is currently a Ph.D. student at NEPO/IFCH/UNICAMP.

Tárcio A. S. Barros holds a Bachelor's degree in Electrical Engineering from the Federal University of Vale do São Francisco (2010), where he graduated with honors. He earned a Master's and a Ph.D. in Electrical Engineering at UNICAMP in 2012 and 2015, respectively. Currently, he is an MS5.1 professor at UNICAMP. He is affiliated with IEEE, the Brazilian Society of Automatics (SBA), and the Brazilian Power Electronics Society (SOBRAEP). He is the main coordinator of the LEPO / LESF-MV.